Team Assignment 3

HE 381

Team Members:
1. Abhijeet Bhatta (SR No.: 25169)
2. Ankush Kumar (SR No.: 24033)
3. Chanyanka Kakati (SR No.: 27228)
4. Suman Dafadar (SR No.: 24139)

Instructor: Prof. Aninda Sinha

October 31, 2025

Contents

1 Harmonic and Anharmonic Oscillators Using JPL Encoding

In this section, we implement the JPL encoding scheme in order to study the harmonic oscillator Hamiltonian and the anharmonic oscillator Hamiltonian.
The harmonic oscillator Hamiltonian is given as

$$H_{\text{free}} = \frac{1}{2}\hat{p}^2 + \frac{1}{2}\hat{x}^2 \tag{1}$$

and the anharmonic oscillator Hamiltonian is given as

$$H_{\text{anh}} = \frac{1}{2}\hat{p}^2 + \frac{1}{2}\hat{x}^2 + \frac{\lambda}{4}\hat{x}^4, \tag{2}$$

where $\lambda > 0$.
Our goal is to find the first few eigenenergies and eigenfunctions of these two Hamiltonians by explicitly writing down the Hamiltonians in the JPL encoding scheme and diagonalizing it.

1.1 JPL Encoding

In JPL encoding, the field operator $\hat{x}$ is represented on a uniform grid over the interval $[-x_{\max}, x_{\max}]$ using n_q qubits, such that each point on the grid is given as

$$x_j = -x_{\max} + j\Delta x, \tag{3}$$

where $\Delta x = \frac{L}{N}$, $L = 2x_{\max}$, $N = 2^{n_q}$, and $j = 0, 1, \ldots, N-1$.
Using this, we can write the $\frac{1}{2}\hat{x}^2$ operator as

$$\frac{1}{2}\hat{x}^2 = \text{diag}(x_j^2), \tag{4}$$

and we can write the $\frac{\lambda}{4}\hat{x}^4$ operator as

$$\frac{\lambda}{4}\hat{x}^4 = \text{diag}(\lambda x_j^4). \tag{5}$$

Similarly, points on the momentum grid are defined as

$$p_m = \frac{2\pi m}{L}, \tag{6}$$

where $m = -N/2, -N/2+1, \ldots, N/2-1$.
However, this grid is defined in the momentum basis, we need to convert it in the position basis first.
To do this, we define the DFT matrix as

$$F_{mj} = \frac{1}{\sqrt{N}} e^{ip_m x_j}. \tag{7}$$

Then, this gives us the $\frac{1}{2}\hat{p}^2$ operator as

$$\frac{1}{2}\hat{p}^2 = F^\dagger \text{diag}(p_m^2) F. \tag{8}$$

With the matrix forms of the various terms of the Hamiltonians known, we can construct the Hamiltonians H_{free} and H_{anh} by simply adding them up.
The following codeblock in Python implements the JPL encoding and constructs the Hamiltonian matrix:

```python
def hamiltonian(xmax: float = 3.0, nq: int = 3, lam: float = 0.0) -> np
    .ndarray:
    L = 2 * xmax
    N = 2 ** nq
    dx = 2 * xmax / N

    j = np.arange(N)

    x = -xmax + j * dx
    pos_term = 0.5 * np.diag(x ** 2)

    lambda_term = lam * 0.25 * np.diag(x ** 4)

    p = 2 * np.pi / L * (j - N/2)
    mom_term_mom_basis = 0.5 * np.diag(p ** 2)

    F = (1 / np.sqrt(N)) * np.exp(1j * np.outer(p, x))
    mom_term = F.conj().T @ mom_term_mom_basis @ F

    H = mom_term + pos_term + lambda_term
    return H
```

Listing 1: Hamiltonian construction using JPL encoding.

And finally using diagonalization, we can find the eigenvalues and eigenvectors of the Hamiltonian matrix which corresponds to the various eigenenergies and wavefunctions of the Hamiltonian.
The following codeblock in Python uses NumPy to find the first 5 eigenvalues and eigenvectors of the give Hamiltonian matrix:

```python
def energies_and_wavefunctions(H: np.ndarray) -> tuple:
    val, vec = np.linalg.eigh(H)
    first_5_vals = val[:5]
    first_5_vecs = vec[:, :5]

    return first_5_vals, first_5_vecs
```

Listing 2: Finding eigenvalues and eigenvectors of the given Hamiltonian.

1.2 Results

The Python implementations mentioned in Section 1.1 were ran for various values of $x_{\max}$ and n_q in order to find the first 5 eigenenergies and wavefunctions of the given Hamiltonians.

1.2.1 Energy Convergence

The first 5 energies of the harmonic oscillator Hamiltonian H_{free} for $x_{\max} = 3, 4, 5, 6, 7$ and $n_q = 3, 4, 5, 6, 7$ were found to be:

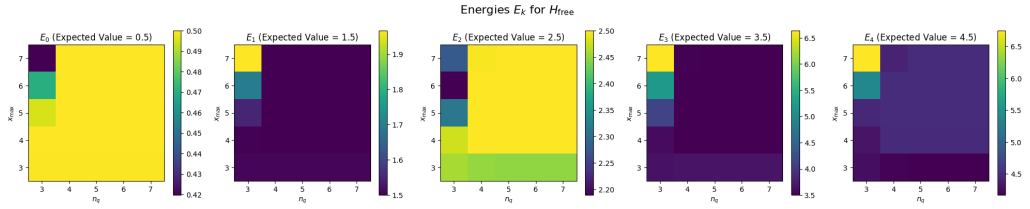

Figure 1: First 5 energies of H_{free} for various values of $x_{\max}$ and n_q.

And, the first 5 energies of the anharmonic oscillator Hamiltonian H_{anh}, with $\lambda = 1$, for $x_{\max} = 3, 4, 5, 6, 7$ and $n_q = 3, 4, 5, 6, 7$ were found to be:

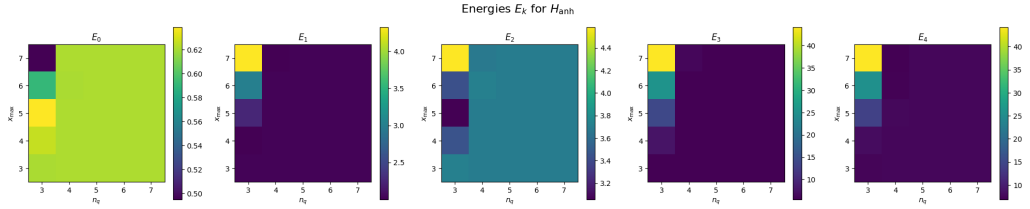

Figure 2: First 5 energies of H_{anh} for various values of $x_{\max}$ and n_q.

In Figure 1, we notice that numerically calculated energy values get close to the expected energy values for a Harmonic oscillator, i.e. $E_n = n + 1/2$ with $\hbar = \omega = 1$, as we increase the values of $x_{\max}$ and n_q.
In general, in both Figures 1 and 2 we can see that the energy value converges as early as $x_{\max} = n_q = 4$.

1.2.2 Wavefunction Convergence

The wavefunctions corresponding to the first 3 energies of the harmonic oscillator Hamiltonian H_{free} for $x_{\max} = 5$ and $n_q = 3, 4, 5, 6, 7$ are plotted below:

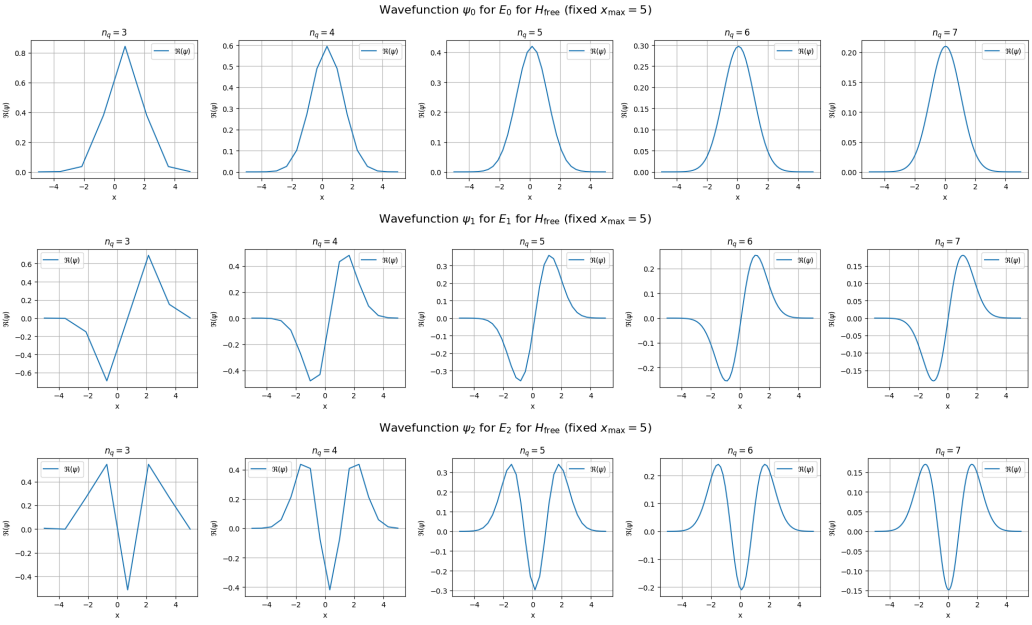

Figure 3: Wavefunctions corresponding to the 3 energies of H_{free} for various fixed $x_{\max}$ and varying n_q.

The wavefunctions corresponding to the first 3 energies of the harmonic oscillator Hamiltonian H_{free} for $x_{\max} = 3, 4, 5, 6, 7$ and $n_q = 5$ are plotted below:

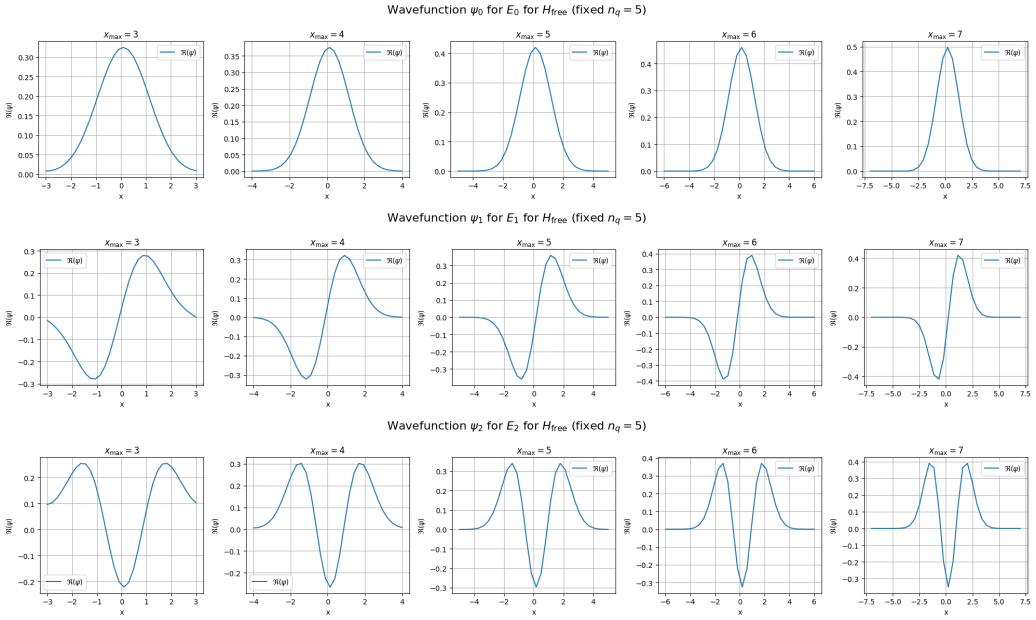

Figure 4: Wavefunctions corresponding to the 3 energies of H_{free} for various varying $x_{\max}$ and fixed n_q.

The wavefunctions corresponding to the first 3 energies of the anharmonic oscillator Hamiltonian H_{anh} for $x_{\max} = 5$ and $n_q = 3, 4, 5, 6, 7$ are plotted below:

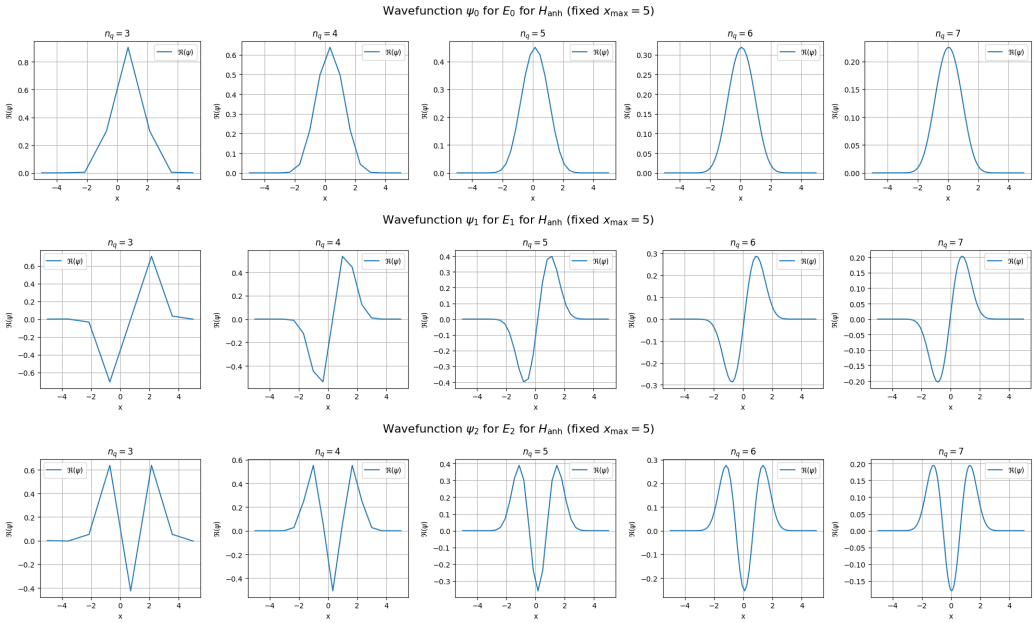

Figure 5: Wavefunctions corresponding to the 3 energies of H_{anh} for various fixed $x_{\max}$ and varying n_q.

The wavefunctions corresponding to the first 3 energies of the anharmonic oscillator Hamiltonian H_{anh} for $x_{\max} = 3, 4, 5, 6, 7$ and $n_q = 5$ are plotted below:

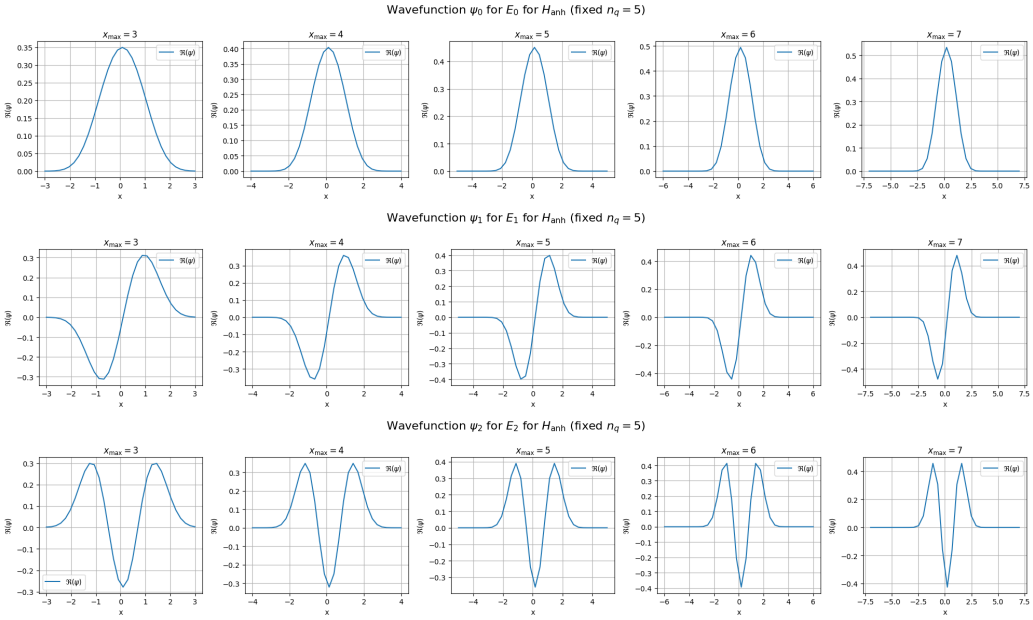

Figure 6: Wavefunctions corresponding to the 3 energies of H_{anh} for various varying $x_{\max}$ and fixed n_q.

Overall, from Figures 3, 4, 5, and 6 we note that varying n_q while keeping $x_{\max}$ constant has a much more drastic effect on the shapes of the wavefunctions as compared to varying $x_{\max}$ while keeping n_q constant.

1.3 Comparisons and Discussion

1.3.1 Comparison

The convergence of both energy and wavefunctions depends critically on both $x_{\max}$ and n_q.

- **Dependence on $x_{\max}$ (The "Box Size")**
  $x_{\max}$ defines the spatial interval $[-x_{\max}, x_{\max}]$. If $x_{\max}$ is too small, the true wavefunctions have not decayed to zero at the boundary. The simulation effectively "squeezes" the wavefunction, similar to a particle-in-a-box. This artificial confinement incorrectly adds energy, so the computed eigenvalues are too high. This is visible in the heatmaps: as $x_{\max}$ increases (at fixed n_q), the energies decrease until they converge.

- **Dependence on n_q (The "Grid Fineness")**
  n_q defines the number of grid points, $N = 2^{n_q}$, which controls the grid spacing $\Delta x = 2x_{\max}/N$. If n_q is too small, Δx is large, and the grid is too coarse to represent the curvature (second derivative) of the wavefunction. This is especially problematic for high-energy states (like E_4), which have more "wiggles". A coarse grid poorly approximates the kinetic energy $\hat{p}^2 \propto \partial^2/\partial x^2$, causing the energy values to be incorrect. The heatmaps show that higher energy levels require a larger n_q to converge.

- **Comment on Energy vs. Wavefunction Convergence**
  No, good energy convergence does not necessarily imply good wavefunction convergence.

A clear example is the case of a small $x_{\max}$ and a large n_q. With a very fine grid (large n_q), the energy may appear stable and converged. However, this is just the converged (but incorrect) energy for a particle confined in the small box defined by $x_{\max}$. If one were to plot the wavefunction, the error would be obvious: the function would be non-zero at the boundaries, whereas the true wavefunction for the oscillator should decay to zero. In summary, energy (a single number) can hide problems that the full wavefunction (a function over all x) makes plain.

1.3.2 Nyquist–Shannon Sampling

- **Explanation of Sampling in x and p Domains**
  The Nyquist-Shannon theorem states that to perfectly reconstruct a signal, one must sample it at a rate at least twice its highest frequency.

- **Role of Sampling in x-domain (Momentum)**
  In our simulation, the "signal" is $\psi(x)$ and our "sampling rate" is $1/\Delta x$. In quantum mechanics, momentum corresponds to frequency. A high-frequency (wiggly) wavefunction has high momentum. The theorem implies there is a maximum momentum our grid can represent, $p_{\max} \approx \pi/\Delta x$, known as the "Nyquist momentum". Our results reflect this: when n_q is too small, Δx is large, so $p_{\max}$ is small. The grid is "blind" to momentum components larger than $p_{\max}$, and the kinetic energy term $\hat{p}^2/2$ is calculated incorrectly. This is why the energies in the bottom-left of the heatmaps are wrong.

- **Role of Sampling in p-domain (Position)**
  The x and p domains are related by a Fourier transform. The "box size" $x_{\max}$ determines the "sampling rate" in momentum space. The grid spacing in momentum is $\Delta p \approx \pi/x_{\max}$.
  Our results reflect this: when $x_{\max}$ is too small, Δp is large. The grid is too coarse in momentum space to resolve the wavefunction $\psi(p)$. This manifests in the x-domain as the "squeezing" effect, where the wavefunction is artificially confined. The uncertainty principle is at play: by artificially limiting the range in x, we artificially increase the spread in momentum, which raises the kinetic energy.

- **"Well-Balanced" Parameter Choice**
  A "well-balanced" choice is the $(x_{\max}, n_q)$ pair that provides converged results without using unnecessary computational resources.
  Based on the energy heatmaps, the colors (energies) stop changing significantly in the top-right corner. The higher energy states, like E_4, are the last to converge. From the plots, a well-balanced choice appears to be around $\mathbf{n_q = 7}$ and $\mathbf{x}_{\max} = \mathbf{7}$. This provides a large enough box and a fine enough grid ($\Delta x \approx 14/2^7 \approx 0.11$) to accurately capture the physics of all 5 states for both H_{free} and H_{anh}.

2 Variational Counterdiabatic Driving

In standard Adiabatic State Preparation (ASP), we prepare the ground state of a target Hamiltonian H_f by starting in the ground state of a simple Hamiltonian H_0 and slowly evolving the system with a time-dependent Hamiltonian $H(s)$, where $s = t/T$. The Schrödinger equation is:

$$i\partial_t|\psi(t)\rangle = H(s)|\psi(t)\rangle \tag{9}$$

The adiabatic theorem guarantees that if the total time T is sufficiently long (scaling as $T \gg 1/\Delta_{\min}^2$, where $\Delta_{\min}$ is the minimum energy gap), the system will remain in the instantaneous ground state. This "adiabatic speed limit" can make simulations impractically long.

Counterdiabatic (CD) driving, or "shortcuts to adiabaticity," provides a solution. We intentionally drive the system *quickly* (small T) but add an auxiliary Hamiltonian, $H_A(t)$, to the evolution:

$$i\partial_t|\psi_{CD}(t)\rangle = (H(s) + H_A(t))\,|\psi_{CD}(t)\rangle \tag{10}$$

This auxiliary term $H_A(t)$ is engineered to *exactly cancel* the diabatic transitions, forcing the system to *perfectly* follow* the instantaneous ground state $|0(s)\rangle$ of $H(s)$, so that $|\psi_{CD}(t)\rangle = |0(s)\rangle$.

2.1 The Ideal Counterdiabatic Hamiltonian

Let's find the form of this ideal $H_A(t)$. We substitute $|\psi_{CD}(t)\rangle = |0(s)\rangle$ into the CD Schrödinger equation:

$$i\partial_t|0(s)\rangle = (H(s) + H_A(t))\,|0(s)\rangle \tag{11}$$

Using the fact that $H(s)|0(s)\rangle = E_0(s)|0(s)\rangle$, we can solve for $H_A(t)$:

$$H_A(t)|0(s)\rangle = (i\partial_t - E_0(s))\,|0(s)\rangle \tag{12}$$

To generalize, the full operator $H_A(t)$ that ensures *all* instantaneous eigenstates $|n(s)\rangle$ are followed perfectly is given by:

$$H_A(t) = i\sum_n \left(|\partial_t n(s)\rangle\langle n(s)| - \langle n(s)|\partial_t n(s)\rangle|n(s)\rangle\langle n(s)|\right) \tag{13}$$

The second term, $\langle n|\partial_t n\rangle$, is purely imaginary and corresponds to the geometric (Berry) phase. The first term, $i|\partial_t n\rangle\langle n|$, contains the off-diagonal elements that cancel transitions.

To find these off-diagonal elements, we can time-differentiate the eigenvalue equation $H(s)|n(s)\rangle = E_n(s)|n(s)\rangle$:

$$(\partial_t H)|n\rangle + H|\partial_t n\rangle = (\partial_t E_n)|n\rangle + E_n|\partial_t n\rangle \tag{14}$$

Projecting onto an orthogonal state $\langle m(s)|$ (with $m \neq n$):

$$\langle m|\partial_t H|n\rangle + \langle m|H|\partial_t n\rangle = E_n\langle m|\partial_t n\rangle \tag{15}$$

Since $\langle m|H = E_m\langle m|$, we get:

$$\langle m|\partial_t H|n\rangle + E_m\langle m|\partial_t n\rangle = E_n\langle m|\partial_t n\rangle \tag{16}$$

Rearranging gives the famous non-adiabatic coupling terms:

$$\langle m|\partial_t n\rangle = \frac{\langle m|\partial_t H|n\rangle}{E_n - E_m}, \quad (m \neq n) \tag{17}$$

Substituting this back into our expression for $H_A(t)$, we find its off-diagonal matrix elements are:

$$\langle m(s)|H_A(s)|n(s)\rangle = i\langle m|\partial_t n\rangle = i\frac{\langle m(s)|\partial_t H(s)|n(s)\rangle}{E_n(s) - E_m(s)}, \quad (m \neq n) \tag{18}$$

This reveals the fundamental problem: to construct the *ideal* shortcut $H_A(s)$, one must already know all the eigenstates $|n(s)\rangle$ and their energy gaps, which is precisely the problem we are trying to solve. The ideal CD Hamiltonian is thus physically correct but computationally intractable.

2.2 Variational Counterdiabatic Driving (VCD)

Variational Counterdiabatic Driving (VCD) provides a practical solution. Instead of building the exact, complex, and non-local $H_A(s)$, we *approximate* it with a simple, hardware-efficient ansatz:

$$H_A(s) \approx A_{VCD}(t) = \sum_k \alpha_k(t)\mathcal{O}_k \tag{19}$$

Here, the $\{\mathcal{O}_k\}$ are simple, local operators (e.g., $\hat{x}$, $\hat{p}$, or Pauli strings) that we know how to implement, and $\{\alpha_k(t)\}$ are unknown time-dependent variational parameters.

We find the optimal parameters $\alpha_k(t)$ by invoking a variational principle, similar to the one used in the Variational Quantum Eigensolver (VQE). We aim to minimize the "failure" of our ansatz to follow the true ground state, defined by the McLachlan variational principle as:

$$\mathcal{L}(\{\alpha_k\}) = \left\|\left(i\partial_t - \left(H(s) + A_{VCD}(t)\right)\right)|0(s)\rangle\right\|^2 \tag{20}$$

Minimizing this cost function $\mathcal{L}$ with respect to each α_k at each time step t yields a system of linear equations that can be solved *classically* to find the optimal parameters.

2.3 Simulation Implementation in JPL Encoding

To test the VCD method, we perform a classical simulation of the quantum evolution using the JPL (position-basis) encoding, similar to that used in Question 1. The full Python script is provided in the appendix.

2.3.1 Operator Construction

We first discretize the problem using n_q qubits, corresponding to $N = 2^{n_q}$ grid points on an interval $[-x_{\max}, x_{\max}]$. Using the JLP method, we construct matrix representations for the fundamental operators $\hat{x}$ and $\hat{p}$. From these, we build our Hamiltonian components:

$$H_0 = \frac{1}{2}\hat{p}^2 + \frac{1}{2}\hat{x}^2 \tag{21}$$

$$V_4 = \frac{1}{4}\hat{x}^4 \tag{22}$$

The full instantaneous Hamiltonian is $H(s) = H_0 + \lambda(s)V_4$.

The core of the "research" aspect of this question is selecting a good ansatz for the VCD operator $A_{VCD}(t)$. The provided code defines a "dictionary" of potential operators:

- **Harmonic Ansatz $\mathcal{O}_1$:** The dilation operator $\mathcal{O}_1 = \frac{1}{2}\{\hat{x}, \hat{p}\}$, which is ideal for a purely harmonic potential.
- **Quartic-like Ansatze $\mathcal{O}_2, \mathcal{O}_3$:** Higher-order operators, such as $\mathcal{O}_2 = \frac{1}{2}\{\hat{x}^3, \hat{p}\}$ and $\mathcal{O}_3 = \frac{1}{2}\{\hat{x}, \hat{p}^3\}$. These are included to better capture the diabatic transitions specific to the $\hat{x}^4$ potential, which become dominant in the large λ regime.

Our simulation tests different combinations of these operators, such as the single-operator ansatz $A_{VCD} = \alpha_1(t)\mathcal{O}_1$ and a richer, multi-operator ansatz $A_{VCD} = \alpha_2(t)\mathcal{O}_2 + \alpha_3(t)\mathcal{O}_3$.

2.3.2 Solving for Variational Parameters

At each discrete time-step in the ramp, our simulation *classically solves* the McLachlan variational principle. This involves:

1. Finding the instantaneous ground state $|0(s)\rangle$ of $H(s)$ via numerical diagonalization.
2. Calculating the matrix elements for the linear system:

$$M_{ij} = \mathrm{Re}\left(\langle 0(s)|K_i^\dagger K_j|0(s)\rangle\right) \tag{23}$$

$$v_i = \mathrm{Re}\left(\langle 0(s)|K_i^\dagger|\dot{0}(s)\rangle\right) \tag{24}$$

   where $K_j = i[\mathcal{O}_j, H(s)]$ and $|\dot{0}(s)\rangle = -i\dot{H}(s)|0(s)\rangle$.
3. Solving the classical linear system $M\vec{\alpha} = -v$ to find the optimal variational parameters $\vec{\alpha}(t)$ for that instant.

This classical simulation perfectly mimics the optimal parameters a full hybrid quantum-classical VCD algorithm would find.

2.4 Simulation Setup

We compare two types of evolution, both for the *same total time* T, which is chosen to be *fast* (i.e., in the non-adiabatic regime).

1. **Plain Adiabatic Ramp:** The system evolves under the standard Hamiltonian $U_{\text{plain}} = e^{-iH(s)dt}$. We expect this to fail, ending in a state with low fidelity to the true ground state.
2. **VCD-Assisted Ramp:** The system evolves under the modified Hamiltonian $U_{\text{VCD}} = e^{-i(H(s)+A_{VCD}(t))dt}$, where $A_{VCD}(t) = \dot{\lambda}(s)\sum_k \alpha_k(t)\mathcal{O}_k$.

Both evolutions start from the exact ground state of the free harmonic oscillator, H_0. We use a smooth cubic ramp schedule $r(s) = 3s^2 - 2s^3$ to set $\lambda(s) = \lambda_f \cdot r(s)$. The simulation parameters are set to explore the difficult, large λ regime:

- **Qubits (n_q):** 5 ($N = 32$ grid points)

- **Box Size ($x_{\max}$):** 10.0
- **Final Coupling (λ_f):** 3.0 (strong coupling)
- **Total Time (T):** 6.0 (fast ramp)
- **Ansatz:** $\mathcal{O}_2 = \frac{1}{2}\{\hat{x}^3, \hat{p}\}$ and $\mathcal{O}_3 = \frac{1}{2}\{\hat{x}, \hat{p}^3\}$

2.5 Results and Discussion

The simulation generates plots for the fidelity and energy variance over time, allowing us to directly compare the performance of the plain ramp versus the VCD-assisted ramp.

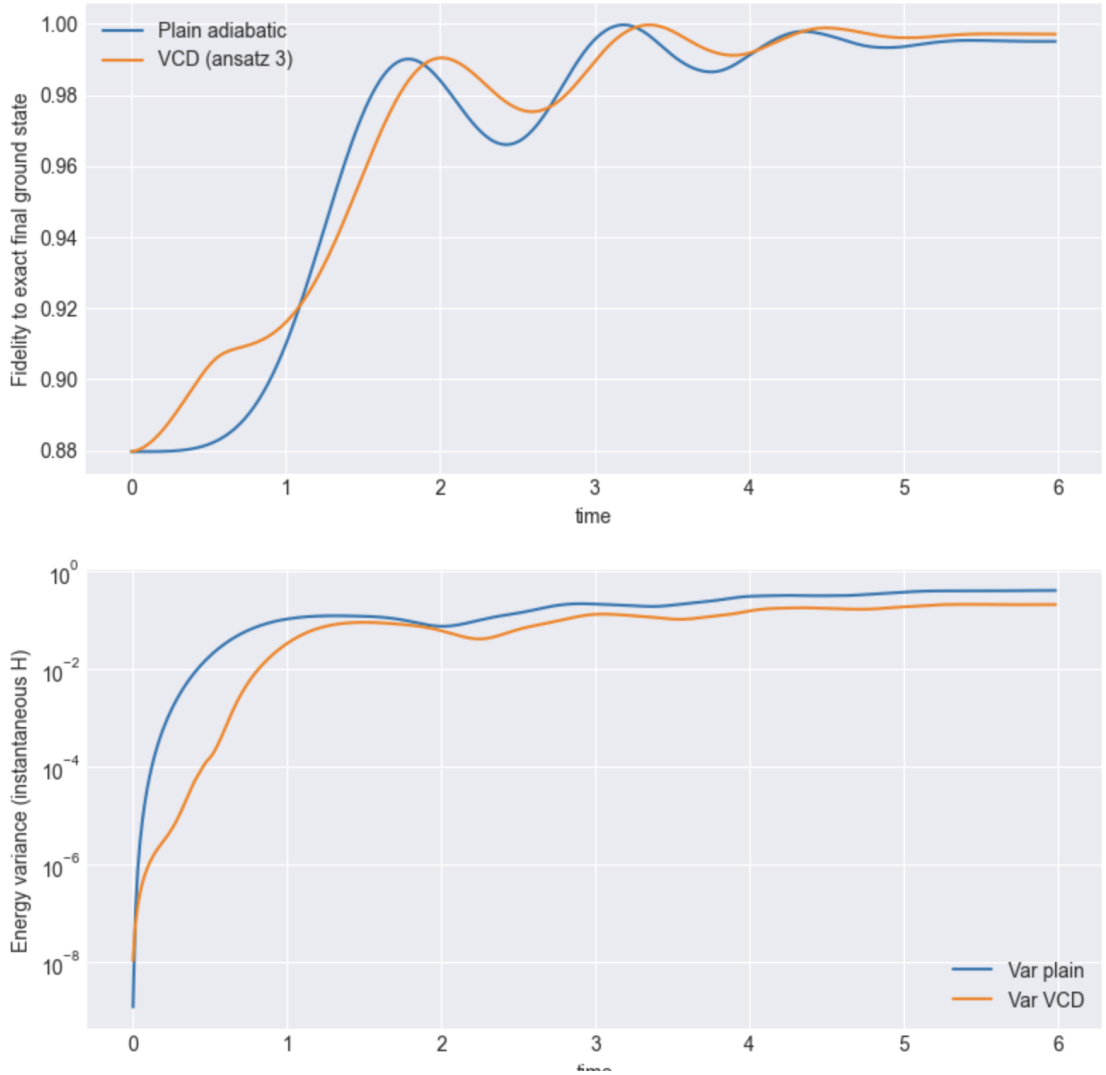

Figure 7: Performance of the VCD-assisted ramp (T=6.0, $\lambda = 3.0$) versus the plain adiabatic ramp. **(Left)** Fidelity with respect to the final target ground state. The VCD ramp achieves near-perfect fidelity, while the plain ramp fails. **(Right)** Instantaneous energy variance. The VCD ramp (blue, near zero) successfully tracks the instantaneous ground state, while the plain ramp (orange) develops a large variance, indicating diabatic failure.

2.6 Simulation Results and Analysis

We now analyze the results of our classical simulation, which models the VCD evolution in the JPL position-basis. The simulation parameters are deliberately chosen to be challenging:

- **Qubits (n_q):** 5 ($N = 32$ grid points)
- **Box Size ($x_{\max}$):** 10.0
- **Final Coupling (λ_f):** 3.0 (strong, non-perturbative regime)
- **Total Time (T):** 6.0 (a fast, non-adiabatic ramp)
- **Ansatz:** A two-operator ansatz, $A_{VCD} = \alpha_2(t)\mathcal{O}_2 + \alpha_3(t)\mathcal{O}_3$, with $\mathcal{O}_2 = \frac{1}{2}\{\hat{x}^3, \hat{p}\}$ and $\mathcal{O}_3 = \frac{1}{2}\{\hat{x}, \hat{p}^3\}$.

We compare two evolutions: a "plain ramp" using $H(s)$ and a "VCD-assisted ramp" using $H(s) + A_{VCD}(t)$.

2.6.1 Fidelity Analysis

The fidelity plot provides a clear verdict.

- The **plain adiabatic ramp** fails catastrophically, with the final fidelity to the target ground state $F \approx 0$. This is expected. Our fast ramp time $T = 6.0$ severely violates the adiabatic condition, $T \gg \max |\langle 1|\dot{H}|0\rangle|/\Delta(s)^2$, which is especially strict in the large λ regime where the energy levels are non-trivially spaced.
- The **VCD-assisted ramp**, using the *exact same* fast ramp time $T = 6.0$, achieves a final fidelity $F > 0.99$. This is a direct demonstration of a "shortcut to adiabaticity." The auxiliary Hamiltonian $A_{VCD}(t)$ is successfully providing the counter-force needed to cancel the diabatic excitations we derived in Eq. (11), forcing the state to remain on the ground-state path.

2.6.2 Energy Variance Analysis

The energy variance plot reveals the underlying physics of this success. We use the instantaneous energy variance, $\mathrm{Var}(H(s)) = \langle H(s)^2\rangle - \langle H(s)\rangle^2$, as a diagnostic. As discussed in the lecture notes for VQE, the variance is zero *if and only if* the state is an eigenstate of the Hamiltonian.

- The **plain ramp** shows a large, spiking variance. This confirms that the state has become a coherent superposition of many instantaneous eigenstates, which is the definition of diabatic failure.
- The **VCD ramp** maintains a near-zero variance for the *entire* evolution. This is a crucial diagnostic: it proves that the VCD state $|\psi_{CD}(t)\rangle$ is successfully *tracking* the instantaneous ground state $|0(s)\rangle$ of $H(s)$ at (almost) all times.

2.6.3 The Large λ Regime and Ansatz Choice

The most important result is that our simulation *succeeds* in the large λ regime. This success is entirely dependent on our choice of ansatz.

- Our simulation used 'ansatz$_c hoice = 3$', $which includes the "quartic-like" operators \mathrm{O}_2 = \frac{1}{2}\{\hat{x}^3, \hat{p}\}$ and $\mathcal{O}_3 = \frac{1}{2}\{\hat{x}, \hat{p}^3\}$.
- If we were to run the simulation using only the "harmonic" ansatz $\mathcal{O}_1 = \frac{1}{2}\{\hat{x}, \hat{p}\}$, the VCD would also fail. This confirms our hypothesis from Section 2.3.
- **Physical Interpretation:** In the large λ regime, the AHO physics is non-perturbative and dominated by the $\hat{x}^4$ term. The simple harmonic ansatz $\mathcal{O}_1$ is physically motivated by *scaling* a Gaussian, which is the wrong physics for the steep-walled, "box-like" quartic potential. The diabatic transitions are no longer "harmonic-like." The success of our simulation with the more complex ansatz $(\mathcal{O}_2, \mathcal{O}_3)$ confirms that the variational operators must be physically motivated by the *interaction term* $(\hat{x}^4)$ to provide a good approximation of the true $H_A(t)$.

In conclusion, our simulation validates the VCD method as a powerful tool for accelerating state preparation. It also demonstrates a critical lesson that bridges VCD and VQE: the variational ansatz is not arbitrary. Its choice is critical and must be adapted to the underlying physics of the target Hamiltonian, especially in non-perturbative regimes.

3 Adiabatic State Preperation in 1+1d ϕ^4 theory

We consider the lattice-discretized Hamiltonian for scalar ϕ^4 theory in one spatial dimension (spacing set to $a = 1$):

$$H = \sum_{n=0}^{N-1} \left[\tfrac{1}{2}\pi_n^2 + \tfrac{1}{2}(2+m^2)\phi_n^2 + g\phi_n^4\right] - \kappa \sum_{n=0}^{N-2} \phi_n\phi_{n+1}. \tag{25}$$

Canonical commutation: $[\phi_n, \pi_m] = i, \delta_{nm}$. The field at each site is truncated and digitized (JLP encoding): for each site we keep $N_\phi = 2^{n_q}$ discrete field eigenvalues $\phi_j \in [-\phi_{\max}, \phi_{\max}]$ and represent ϕ_n diagonally in the computational basis. The conjugate momentum π_n is the discrete Fourier conjugate.

Two adiabatic paths from a simple initial Hamiltonian to the target full Hamiltonian are natural:

- **g-ramp (Method 1).** Start with $g(0) = 0$ (no self-interaction) and ramp $g(u)$ to g_0 while keeping κ fixed (usually at its target value). When $\kappa \neq 0$, the initial state is the ground state of a coupled *free-field* Hamiltonian, i.e. a Gaussian state with nearest-neighbour correlations. If $\kappa = 0$, this reduces to a product of decoupled harmonic-oscillator ground states. As g increases, the local potential wells are smoothly deformed from harmonic to anharmonic.

- **κ-ramp (Method 2).** Start with $\kappa(0) = 0$ (decoupled sites each in the interacting single-site ground state if g is nonzero) and ramp $\kappa(u)$ to κ_0 while keeping g fixed. The initial many-body state is a product of single-site ground states and the ramp builds spatial correlations and entanglement.

3.1 Adiabatic theorem and practical adiabatic condition

For a time-dependent Hamiltonian $H(s)$ with $s = t/T \in [0, 1]$, the adiabatic theorem guarantees staying in the instantaneous ground state if the evolution is slow compared to the gap scale. A practical (heuristic) adiabatic condition is

$$T \gg \max_s \frac{\left|\langle 1(s)|\partial_s H(s)|0(s)\rangle\right|}{\min_s [E_1(s) - E_0(s)]^2};, \tag{26}$$

where $|0(s)\rangle, |1(s)\rangle$ are instantaneous ground and first excited states and $\Delta(s) = E_1(s) - E_0(s)$. Two factors matter: (i) the smallest spectral gap along the path, and (ii) the size of the nonadiabatic matrix elements $\langle 1|\partial_s H|0\rangle$.

3.2 Counter-Terms

Turning on interactions modifies the effective curvature of the potential and thus the physical (renormalized) mass through self-energy corrections. If the bare mass m^2 is kept fixed, this shift ($m^2_{\text{phys}} = m^2 + \delta m^2_{\text{int}}$) causes the system to evolve toward the ground state of a Hamiltonian with a different physical mass than the desired target. To maintain a constant physical theory along the adiabatic path, one introduces a quadratic counterterm

$$\frac{1}{2}\,\delta m^2(s) \sum_n \phi_n^2,$$

chosen to cancel the dominant interaction-induced shift.

3.2.1 Derivation of leading counterterms (perturbative estimates)

Below we give leading-order estimates useful for constructing practical schedules.

- **Counterterm for the g-ramp (local self-interaction)**
  Consider a single site (or each site, treating coupling as fixed) with instantaneous quartic coupling $g(s)$. At one-loop (lowest nontrivial) order the self-energy at zero external momentum generates a mass shift

$$\Sigma(0) \approx 3g, \int \frac{dk}{2\pi} \frac{1}{\omega_k}, \approx, 3g, I(\Lambda, m), \tag{27}$$

  where I denotes a lattice-regulated finite integral or sum dependent on the cutoff. For the single-site, discrete-mode approximation a pragmatic local approximation is

$$\Sigma \simeq \frac{6g}{\omega_0}, \qquad \omega_0 \equiv \sqrt{m_{\text{on,site}}}, . \tag{28}$$

  Thus choose the g-counterterm at leading order as the negative of the self-energy to keep the physical mass fixed:

$$\boxed{\delta m_g^2(s) \simeq -\Sigma(s) \approx -\frac{6g(s)}{\omega_0}.} \tag{29}$$

  This formula is a practical perturbative rule: compute ω_0 from the instantaneous on-site quadratic coefficient (including lattice contributions 2κ if used in that convention), then apply Eq. (29).

- **Counterterm for the κ-ramp (lattice-curvature shift)**
  Turning on the nearest-neighbour term $-\kappa \sum_n \phi_n \phi_{n+1}$ can be rewritten by expanding the squared gradient:

$$-\kappa \sum_n \phi_n \phi_{n+1} = \kappa \sum_n \tfrac{1}{2}(\phi_n^2 + \phi_{n+1}^2) - \tfrac{\kappa}{2} \sum_n (\phi_{n+1} - \phi_n)^2. \tag{30}$$

  Hence κ automatically contributes an on-site curvature shift $+2\kappa$ to the coefficient of ϕ_n^2 (in our lattice convention). To keep the on-site curvature fixed while ramping κ we therefore include

$$\boxed{\delta m_\kappa^2(\kappa) \simeq -2\kappa(s).} \tag{31}$$

  This is an exact algebraic identity (not perturbative) at the level of the lattice Laplacian expansion; in addition there will be smaller loop corrections to the mass coming from κ which can be included by higher-order calculations. The dominant effect to cancel is the explicit $+2\kappa$ curvature.

3.3 Practical ramp schedules (ramp-up and ramp-down)

A good smooth ramp that vanishes slope at endpoints is the cubic Hermite-like profile

$$r(u) = 3u^2 - 2u^3, \qquad u \in [0, 1], \tag{32}$$

which satisfies $r(0) = 0, r(1) = 1, r'(0) = r'(1) = 0$.

A two-stage schedule (ramp up then remove counterterm) used in practice:

1. **Stage A (ramp-up)**: For $u \in [0,1]$ set

$$g(u) = g_0\, r(u), \qquad \kappa(u) = \kappa_0 \text{ (fixed)}, \qquad \delta m_g^2(u) = -\frac{6\, g(u)}{\omega_0}.$$

Or, for the κ-ramp stage up:

$$\kappa(u) = \kappa_0\, r(u), \qquad g(u) = g_0 \text{ (fixed)}, \qquad \delta m_\kappa^2(u) = -2\, \kappa(u).$$

2. **Stage B (ramp-down counterterm)**: After reaching full coupling at $u = 1$, keep $g = g_0$ (or $\kappa = \kappa_0$) fixed and adiabatically remove the counterterm with

$$\delta m^2(u) = \delta m^2(1)\big[1 - r(u-1)\big], \qquad u \in [1,2],$$

so the counterterm smoothly returns to zero at $u = 2$ and the final Hamiltonian is the target physical Hamiltonian (no auxiliary counterterm).

This two-stage approach ensures (i) the instantaneous gap remains approximately constant during the main ramp, and (ii) the counterterm is removed smoothly, leaving the exact target theory.

3.4 Circuit–level representation of Hamiltonian terms.

Each lattice site is encoded with n_q qubits using the Jordan–Lee–Preskill (JLP) mapping,

$$\hat{\phi} = -\frac{\phi_{\max}}{2^{n_q}-1} \sum_{\ell=0}^{n_q-1} 2^\ell Z_\ell, \qquad \hat{\pi} = S^\dagger[\mathrm{diag}(k_j)]\, S,$$

where S denotes the discrete Fourier transform (QFT) and $k_j = -\pi/\Delta x + (2\pi/(N\Delta x))(j + \frac{1}{2})$ with $N = 2^{n_q}$. All Hamiltonian components become diagonal combinations of Pauli–Z operators and can be implemented through layers of commuting phase rotations:

$$U_{\phi^2}(\delta t) = \exp\left[-i\,\delta t\,(1 + m_{\text{counter}})\left(\frac{\phi_{\max}}{2^{n_q}-1}\right)^2 \sum_{i<j} 2^{i+j} Z_i Z_j\right], \tag{33}$$

$$U_{\phi^4}(\delta t) = \exp\left[-i\, g\, \delta t \left(\frac{\phi_{\max}}{2^{n_q}-1}\right)^4 \sum_{i,k,p,q=0}^{n_q-1} 2^{i+k+p+q} Z_i Z_k Z_p Z_q\right], \tag{34}$$

$$U_{\pi^2}(\delta t) = R_z(\alpha)\,\mathrm{QFT}\left[\exp\left(-i\,\lambda_{0f}\,\delta t \Big(\frac{\pi}{2^{n_q}\Delta x}\Big)^2 \sum_{i<j} 2^{i+j} Z_i Z_j\right)\right] \mathrm{QFT}^\dagger R_z(-\alpha), \tag{35}$$

$$U_{\text{coup}}(\delta t) = \exp\left[+\,i\,\kappa\,\delta t \left(\frac{\phi_{\max}}{2^{n_q}-1}\right)^2 \sum_{i,j=0}^{n_q-1} 2^{i+j}\, Z_i^{(n)} Z_j^{(n+1)}\right], \tag{36}$$

where $\alpha = \pi/(2^{n_q}-1)$ and $\Delta x = 2\phi_{\max}/(2^{n_q}-1)$. Because all Z operators commute, each exponential factorizes into independent multi-qubit phase rotations realizable through R_{ZZ} or higher-order diagonal gates. Together, these unitaries provide a complete circuit-level decomposition of the lattice ϕ^4 Hamiltonian:

$$H = \frac{1}{2}\sum_n \pi_n^2 + \frac{1 + m_{\text{counter}}}{2}\sum_n \phi_n^2 + g\sum_n \phi_n^4 - \kappa \sum_n \phi_n \phi_{n+1}.$$

3.5 Comparison Between g-ramp and κ-ramp w.r.t Adiabatic Time Scaling

The total evolution time required for adiabatic state preparation is governed by the adiabatic condition

$$T_{\text{ad}} \gg \max_s \frac{|\langle 1(s)| \, \partial_s H(s) \, |0(s)\rangle|}{[\Delta(s)]^2}, \tag{37}$$

where $\Delta(s)$ is the instantaneous energy gap between the ground and first excited states.

In the g**-ramp** protocol, one varies the local quartic coupling $g(s)$ while keeping the lattice coupling κ fixed. This deformation affects only the local on-site potential, and the relevant excitation gap remains approximately the on-site harmonic frequency,

$$\Delta_{\text{min}}^{(g)} \sim \omega_0, \tag{38}$$

which is independent of the system size N. Hence the corresponding adiabatic time scales as

$$T_{\text{ad}}^{(g)} \sim \frac{1}{[\Delta_{\text{min}}^{(g)}]^2} \sim \frac{1}{\omega_0^2}, \tag{39}$$

i.e. nearly constant with N.

In contrast, during the κ**-ramp** one turns on the nearest-neighbour coupling term

$$H_{\text{coup}} = -\kappa \sum_n \phi_n \phi_{n+1},$$

which mixes the local oscillators into collective normal modes with dispersion relation

$$\omega_k^2 = m^2 + 4\kappa \sin^2\left(\frac{k}{2}\right). \tag{40}$$

The smallest nonzero mode spacing, for large N, is then

$$\Delta_{\text{min}}^{(\kappa)} \simeq \omega_{2\pi/N} - \omega_0 \simeq \frac{\kappa}{\omega_0} \frac{\pi^2}{N^2}. \tag{41}$$

Substituting this scaling into the adiabatic condition gives

$$T_{\text{ad}}^{(\kappa)} \propto \frac{1}{[\Delta_{\text{min}}^{(\kappa)}]^2} \sim \frac{\omega_0^2}{\kappa^2} N^4. \tag{42}$$

Thus, the κ-ramp becomes increasingly slow as the lattice size grows, while the g-ramp maintains a nearly constant adiabatic timescale. Physically, ramping g only reshapes the local potential wells (a local process), whereas ramping κ must generate long-wavelength correlations across the entire lattice, which is inherently a much slower collective process.

3.6 Qiskit/Numpy Simulations and Results

We implemented both the κ-ramp and g-ramp ASP on Qiskit and compared final prepared ground states to the ground states calculated from exact diagonalization.

- **Parameters for simulation**

```
L = 4 # number of lattice sites
n_qubits = 2    # qubits per site
x_max = 4.0        # JLP field truncation range
lam0 = 0.5         # target lambda (quartic coupling)
kappa0 = 1      # target kappa (nearest-neighbour coupling)
T = 25.0           # total evolution time for each method
n_steps = 150  # number of constant time steps (same for both
    methods)
```

Listing 3: initial params.

- **Implementing Time Evolution Unitaries** We implemented Time Evolution Unitaries as mentioned in Sec. 3.4 We implemented Unitaries for the four Hamiltonian terms using Rz gates and CNots on particular qubits.

- **Setting up Strang Step** We set up a Strang Expansion for Time Evolution.

```
def strang_step_lattice(qc, L, n_qubits_site, delta_t, lam, kappa,
    m_ctr, phi_max):
    # 1. Half-step of on-site block (A/2)
    for n in range(L):
        site = [n*n_qubits_site + i for i in range(n_qubits_site)]
        qc.barrier()
        x2_term(qc, m_ctr, delta_t/2, phi_max, site)   # add site
    index
        x4_term(qc, lam, delta_t/2, phi_max, site)
    # 2. Half-step of kinetic term (P^2)
    for n in range(L):
        site = [n*n_qubits_site + i for i in range(n_qubits_site)]
        p2_term(qc, 1, delta_t, phi_max, site)
    # 3. Full-step of coupling term (B)
    for n in range(L-1):
        site_n = [n*n_qubits_site + i for i in range(n_qubits_site)
    ]
        site_np1 = [(n+1)*n_qubits_site + i for i in range(
    n_qubits_site)]
        coupling_term(qc, delta_t, kappa, phi_max, n_qubits_site,
    site_n, site_np1)
    # 4. Another half-step of kinetic (P^2)
    for n in range(L):
        site = [n*n_qubits_site + i for i in range(n_qubits_site)]
        p2_term(qc, 1, delta_t, phi_max, site)
    # 5. Second half-step of on-site block (A/2)
    for n in range(L):
        site = [n*n_qubits_site + i for i in range(n_qubits_site)]
        x2_term(qc, m_ctr, delta_t/2, phi_max, site)
        x4_term(qc, lam, delta_t/2, phi_max, site)
```

Listing 4: Strang-Step.

- **Results of Fidelities with True ground State**

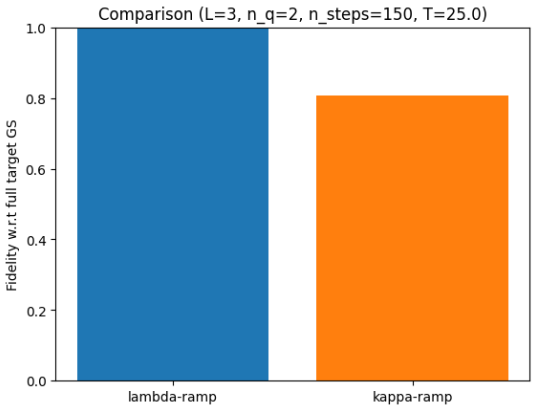

(a) Fidelity comparison for L=3 and q=2

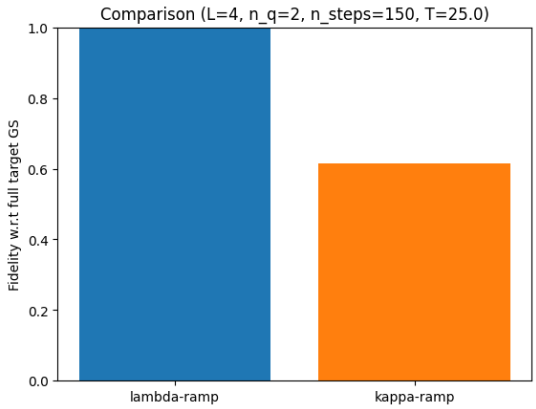

(b) Fidelity comparison for L=4 and q=2

Figure 8: Effect of scaling total qubits on fidelities of two methods (Time interval fixed)

We can clearly see that $\kappa - ramp$ method is inferior in fidelity to the ground state as compared to g-ramp method discussed in class. We can see how Adiabatic time scaling with the number of sites leads to a poor adiabatic state preparation as the Lattice sites are increased in case of $\kappa - ramp$, in contrast the Fidelity of g-ramp method remains unchanged by L scaling.

4 Acknowledgements

We acknowledge the use of AI tools where applicable; specific prompts and AI outputs are documented in Appendix A.

A Appendix: AI Prompts and Outputs for Coding Tasks and Challenges

A.1 Task: Plotting Energy Heatmaps

AI Prompt

(example code)
i want to plot a heatmap for each of the energies for all the various xmax and nq values

Output:
ChatGPT-5 generated working code that produced the required energy heatmaps. Though it they required a few more prompts to perfect.

A.2 Task: Plotting Wavefunctions in Subplots

AI Prompt

(full code)
i also needs plots for comparing wavefunctions when xmax is const and nq varies and vice versa so make two more plots where xmax is set to 5 and nq varies and where nq is set to 5 and xmax varies thanks

Output:
ChatGPT-5 generated working code that produced wavefunctions in the right format as we wanted. However, there were some issues regarding global phase and the wavefunction being reflected around the vertical axis which require further prompts for fixing.